7B.8

EVOLUTION OF HUMIDITY AND CONVECTION PRIOR TO MJO ONSET AND THEIR SENSITIVIES TO UPPER-TROPOSPHERIC EQUATORIAL WAVE DYNAMICS

SCOTT W. POWELL AND ROBERT A. HOUZE, JR.
Department of Atmospheric Sciences, University of Washington, Seattle, Washington

1. INTRODUCTION

Intraseasonal variability in tropical convection was first noted by Madden and Julian (1971, 1972) using time series of outgoing longwave radiation and vertical profiles of zonal wind, temperature, and geopotential. Such variability, which occurs on timescales of 20 to 100 days, is now known as the Madden-Julian Oscillation (MJO) and is further described by Zhang (2005). The MJO is often identified by its cloud pattern of widespread, eastward propagating convection that originates over the Indian Ocean or tropical west Pacific. The area of convection propagates at about 5 m s^{-1}. During boreal winter, MJO-related convection is often located near the equator; however, during boreal summer, widespread and slowly eastward propagating convection is observed farther poleward in the upward branch of the Indian monsoon. Objectively, indices used to identify the MJO heavily depend on circulation anomalies at 200 hPa and/or 850 hPa (Wheeler and Hendon 2004; Ventrice et al. 2013) and less so on anomalies of outgoing longwave radiation (OLR). Despite over 40 years of study on the MJO, unknown are the dynamics explaining how initial onset of widespread, organized convection occurs and how the convection propagates eastward once it becomes established.

Several hypotheses have been offered to explain how initial convective onset of an MJO event occurs. Knutson and Weickmann (1987) suggested that circumnavigating anomalies of velocity potential were connected to MJO convective onset. A Kelvin wave excited by one MJO event could propagate eastward around the globe and excite another MJO event once it reached the Indian Ocean. Such circumnavigating features have been shown to exist in individual cases (Matthews 2008, Gottschalck et al. 2013, Straub 2013) and in composites of several MJO cases (Seo and Kim 2003, Kiladis et al. 2005, Straub 2013, Adames and Wallace 2014).

Bladé and Hartmann (1993) suggested that no clear relationship exists between upper tropospheric velocity potential and formation of convection in the lower troposphere. They proposed a cloud-humidity feedback mechanism, called “discharge-recharge”, in which convective clouds gradually grow deeper over several weeks, depositing moisture into progressively higher levels of the troposphere and making conditions favorable for convection to grow deeper. Several studies afterward supported the hypothesis (e.g. Kemball-Cook and Weare 2001, Benedict and Randall 2007). Such composite studies indicated that the vertical build-up of humidity and moist static energy occurred over 10-20 days.

Powell and Houze (2013, hereafter PH13) rejected “discharge-recharge” as a likely mechanism for MJO convective onset for events observed during the Dynamics of the Madden-Julian Oscillation (DYNAMO) and the Atmospheric Radiation Measurement (ARM) Program Madden-Julian Oscillation Experiment (AMIE) field campaigns (Yoneyama et al. 2013). They showed that the build-up of convective echoes and humidity prior to MJO convective onset for each of three cases observed occurred on timescales of one week or less. Furthermore, if they composited the three observed events together, the evolution of the vertical extent of humidity anomalies and convective depth appeared as if they gradually increased for two or more weeks. Thus, PH13 strongly cautioned the use of composite studies to make conclusions about the dynamics responsible for MJO convective onset.

Conclusions in PH13 were based on observations obtained in the central equatorial Indian Ocean at Gan Island (0.69°S, 73.15°E). The current study seeks to confirm that the variability observed in convection and profiles of zonal wind, temperature, and humidity during DYNAMO/AMIE near Gan are consistent with the large-scale environment. We will then examine the three-dimesional structure and propagation history of upper-tropospheric anomalies and develop a hypothesis for

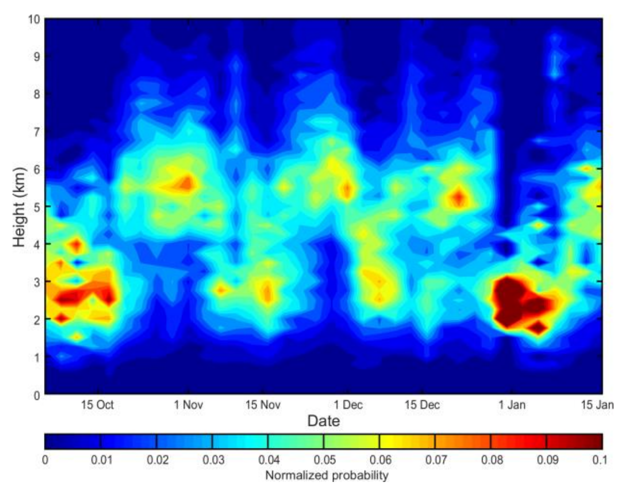

Figure 1: Time series of the normalized probability distribution function of 20 dBZ echo top heights for convective elements observed by TRMM composited for data available between 3°N, 3°S, 68°E, and 78°E. Each time step represents a three-day long mean.

Corresponding Author Address: S. W. Powell, Department of Atmospheric Sciences, University of Washington, Box 351640, Seattle, Washington, 98195, USA (spowell@atmos.uw.edu)

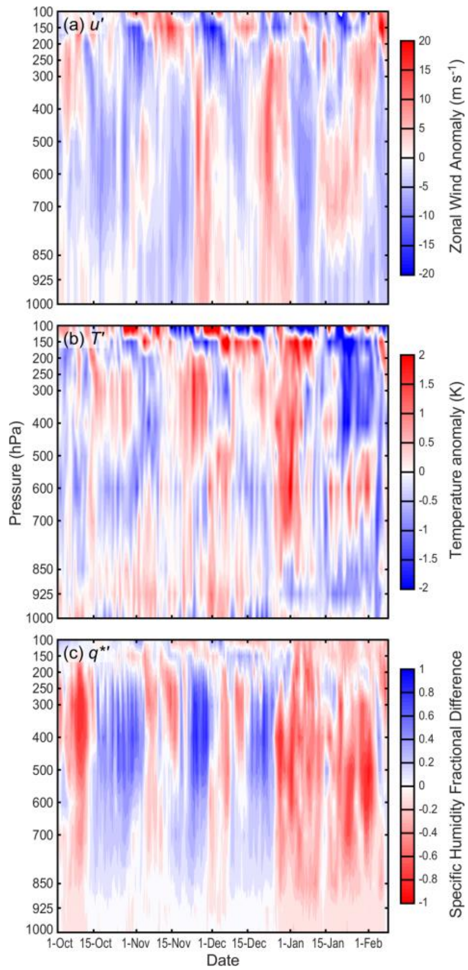

Figure 2: Time series of anomalies of a) zonal wind, b) temperature, and c) the fractional difference of specific humidity from its mean as represented in ERA-I reanalysis from 1 October – 9 February. The seasonal cycle is not removed in this figure.

how upper-tropospheric dynamics affect widespread, organized convection associated with an MJO.

2. DATA

Data from the precipitation radar (PR) aboard the Tropical Rainfall Measuring Mission (TRMM) satellite (Kummerow et al. 1998) are used to compare ground-based radar data to echoes seen throughout the Indian Ocean during DYNAMO. We use version 7 TRMM 2A25 and 2A23 products, which contain reflectivity and rain-type classification (Awaka et al. 1997). Data were mapped onto a 0.05° by 0.05° Cartesian grid with 0.25 km vertical spacing following Houze et al. (2007).

Rawinsonde data is compared to large-scale environmental fields as seen in ERA-Interim reanalysis (ERA-I, Dee et al. 2011) on a 0.75° by 0.75° grid. Reanalysis fields are available at 6 h intervals, and output at 1000, 925, 850, 700, 600, 500, 400, 300, 250, 200, 150, and 100 hPa is used. A low-pass Fourier filter was run on temperature fields to remove strong diurnal variability in the reanalysis. The mean seasonal cycle from 1979-2011 is first removed for fields illustrated in Section 4.

3. COMPARISON OF FIELD OBSERVATIONS TO LARGE-SCALE ENVIORNMENTAL CONDITIONS

3.1 Convective Echoes

Figure 1 depicts a time series, derived from TRMM PR, of the normalized vertical profiles of the probability distribution function of 20 dBZ echo top height for echoes classified as convective. Echo top heights are computed in the same manner as in PH13. The time series is composited in a region between 3°S, 3°N, 68°E, and 78°E, which is centered near Gan. One time step on the abscissa represents three days, and each profile is normalized by the total number of 20 dBZ echo tops observed within each three-day period.

Three periods of heightened convection are noted. The modal distribution (represented by warm colors) of convective 20 dBZ echo tops ranges between 4-7 km during periods of enhanced convection, while the modal distribution remains below 4 km during suppressed periods. The three periods of deep convection coincide with the MJO events observed by ground-based radar during DYNAMO (see PH13, Fig. 8a for comparison).

3.2 Zonal Wind, Temperature, and Humidity Profiles

Rawinsonde data at Gan Island only represents the environmental conditions near the field site. Large-scale fields must be evaluated to determine the representativeness of the field campaign data to large-scale conditions. Figure 2 shows time series of zonal wind (u'), temperature (T'), and humidity ($q^{*'}$) anomalies as represented in ERA-I composited within the same box used for Figure 1. The evolution of anomalies over a large portion of the central, equatorial Indian Ocean are consistent with that observed directly at Gan (see PH13, Figure 7 for comparison). 25-30 day variability is noted in zonal wind anomalies above 300 hPa and is maximum near 150 hPa. Such variability is also seen in temperature and humidity anomalies between 500 and 200 hPa. Three distinct periods of warming and moistening are seen between 500 and 200 hPa, and westerly wind bursts follow each of the three events near the end of October, November, and December.

4. THREE-DIMENSIONAL STRUCTURES OF ZONAL WIND, TEMPERATURE, AND HUMIDITY ANOMALIES

4.1 Time-Longitude Analysis

The time series seen in Figure 2 only show the evolution of upper-tropospheric structure at one point in an Eulerian sense. However such observations do not provide information about the life cycle of the anomalies as they develop in and/or propagate through the tropics. As many prior studies have shown (Section 1), anomalies of velocity potential, which are dominated by u' because anomalies of meridional wind near the equator are relatively small (Johnson and Ciesielski 2013, Powell and Houze 2013), have been noted to

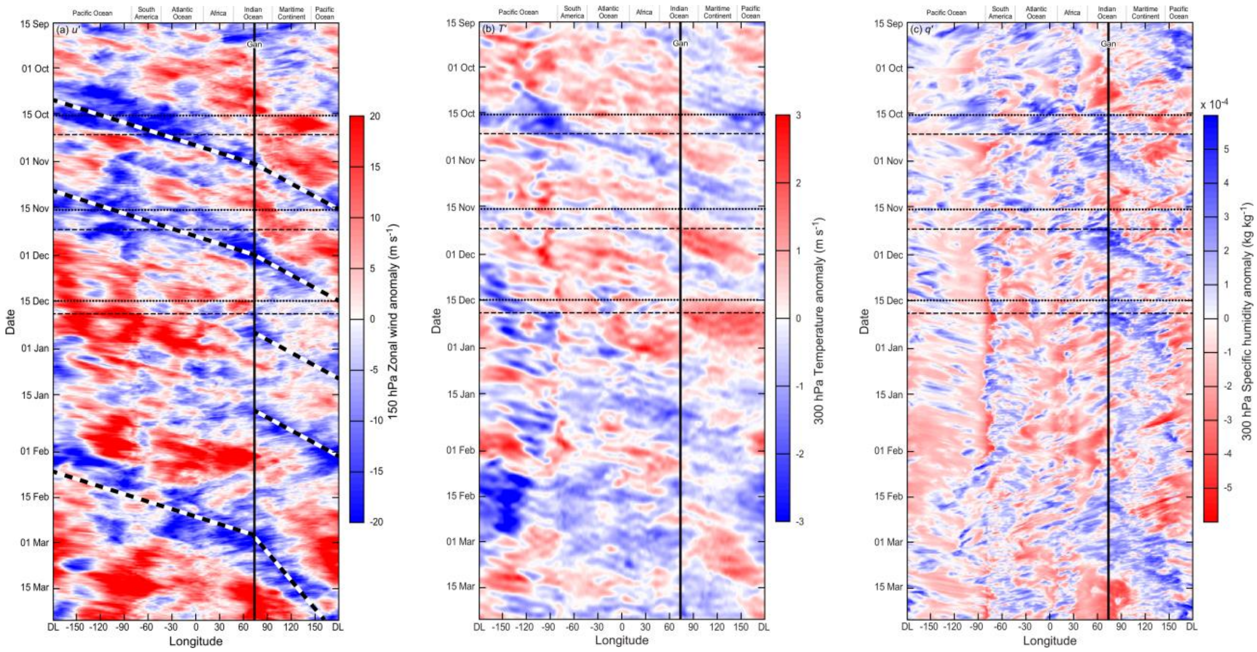

Figure 3: Time-longitude plots of anomalies of a) 150 hPa zonal wind, b) 300 hPa temperature, and c) 300 hPa specific humidity. The solid vertically oriented black line represents the longitude of Gan. Dotted black horizontal lines represent the date of the first MCS observed during each LCE. Dashed black lines indicate the date of the maximum in the 20-40 day filtered precipitation time series. Black and white dashed lines in (a) follow low-wavenumber easterly anomalies.

propagate into the Indian Ocean region from the west. Figure 3 contains time-longitude (Hovmöller) diagrams of 150 hPa u', 300 hPa T' and 300 hPa specific humidity anomalies (q'). For each, values are averaged within three latitudinal degrees of the equator. The vertical, bold black line in each represents the longitude of Gan. Each set of horizontal black lines represents a large-scale convective event (LCE) of the MJO observed during DYNAMO. Dotted, horizontal, black lines represent the date of the first MCS observed near Gan for each LCE. The dashed lines represent the dates of filtered precipitation maxima obtained by Fourier filtering the raw radar-estimated rainfall with a 20-40 day bandpass range. While over the Atlantic Ocean and Africa, u' and T' are nearly in phase with each other. This is particularly true at approximately 15 September-15 October, 5-15 November, 1-10 December, and 1-10 February. In phase temperature and zonal wind anomalies are consistent with an equatorial free Kelvin wave structure such as that seen in Frierson (2007).

For an observer at a single location, an upper-tropospheric divergence anomaly (negative velocity potential anomaly) associated with an eastward propagating disturbance exists after a westerly anomaly passes and before an easterly anomaly passes. The black and white lines in Figure 3a follow low-wavenumber easterly anomalies. The lines represent a phase speed of 15 m s^{-1} to the west of Gan and 10 m s^{-1} east of Gan, except during the MJO event observed during February and March 2012, during which the anomalies propagated eastward near 3.5 m s^{-1} after widespread convection became established. The phase speeds of the zonal wind and associated divergence anomalies match those of OLR anomalies that project onto a Kelvin mode (Wheeler and Weickmann 2001). The phase speed slows over the Indian Ocean as expected because convection becomes coupled with the large-scale equatorial wave (Kiladis et al. 2009). When coupling occurs, 300 hPa T' becomes in quadrature with 150 hPa u' and in phase with the 150 hPa divergence. Such a relationship between zonal wind and temperature is the structure of the MJO as shown by Kiladis et al. (2005), and it is part of a second baroclinic structure that is a response to the upper-tropospheric heating anomaly induced by formation of widespread stratiform. While the temperature anomalies of the free Kelvin mode are dominated by adiabatic processes, we speculate that temperature anomalies associated with the forced Kelvin response over the Indian Ocean or tropical West Pacific may be caused by enhanced radiative heating of stratiform and non-precipitating anvil cloud. It may also be attributed to compensating downward motion outside of convective ascent regions, an idea promoted by Gray (1973).

The 300 hPa humidity anomaly seen in Fig. 3c does not propagate into the Indian Ocean from the west. A positive humidity anomaly does propagate into the MJO convective onset region in late October, but it arrives at the end of the first LCE. The humidity anomalies form in place where convection is first observed and are likely caused by some combination of cloud moistening processes and large-scale advection.

While 25-30 day variability in 850 hPa zonal wind and temperature was observed where MJO-related convection occurred, such lower-tropospheric anomalies formed where convection developed and did not

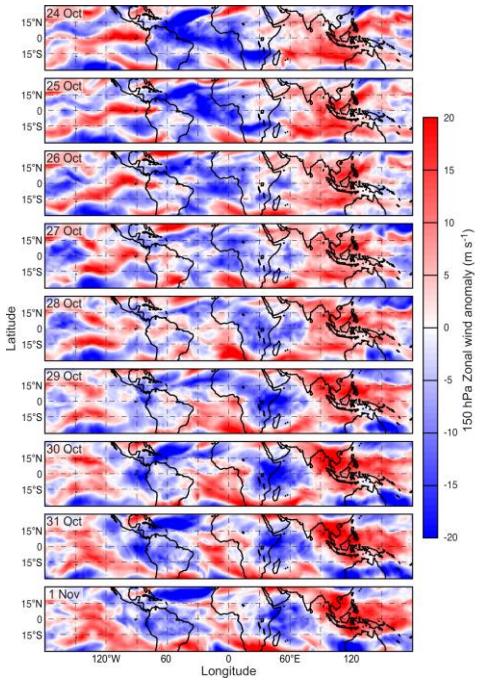

Figure 4: Plan views of ERA-I zonal wind anomalies between 30N and 30S from 24 October – 1 November.

propagate into the region of convective onset from elsewhere (not shown).

For each of the MJO cases observed during DYNAMO, widespread, organized convection first occurred over the central Indian Ocean, but it did not occur (dotted black lines in Fig. 3) until westerly zonal wind anomalies and positive temperature anomalies arrived. Each LCE observed during DYNAMO occurred only when a negative velocity potential anomaly in the upper-troposphere reached the central, equatorial Indian Ocean. In fact, Straub (2013) reports that prior to ~90% of MJO convective events, some precursor signal in the upper-tropospheric zonal wind field can be detected upstream of the region of MJO convective onset. However during January 2012, a pair of zonal wind anomalies moved from the Indian Ocean into the maritime continent and equatorial west Pacific Ocean, a behavior that in Fig. 3a is otherwise indicative of MJO occurrence. No MJO convective onset was observed during January. Fig. 2 shows that extremely dry air was present over the central Indian Ocean during the first half of January. The dry air was advected into the region from the Arabian Peninsula and Africa. The dry air may have prevented a convectively active MJO from taking place. Therefore, a negative upper-tropospheric velocity potential anomaly may be a necessary but not sufficient condition for MJO convective onset.

4.2 *Plan Views*

The Hovmöller diagrams in Fig. 3 show the zonal propagation history of anomalies near the equator, but they do not depict the meridional extent of the anomalies. Figure 4 is a plan view of the 150 hPa zonal wind anomalies during 24 October – 1 November, near the end of the LCE observed at Gan in October 2011. On 24 October, a large region of westerly anomalies was present from 60°E to 150°E, and easterly anomalies extended from eastern Africa to South America. On 25-26 October, a meridionally narrow area of easterly zonal wind anomalies entered the Indian Ocean; it was confined mostly within 5° of the equator. Over the next several days, the easterly anomaly moved slowly eastward and expanded meridionally, so that by 1 November it spanned roughly 25°N to 25°S in the western Indian Ocean. The center of the divergence anomaly was located between the large-scale westerly and easterly anomalies and moved from between 30°E and 60°E on 24 October to about 90°E on 1 November. Though not shown, negative temperature anomalies progressed into the Indian Ocean during the same period in a similar manner. A meridionally narrow region of negative temperature anomalies first appeared in the western and central equatorial Indian Ocean. As the anomaly marched eastward it expanded poleward to extend between 15°N and 15°S by 1 November. The arrival of negative temperature anomalies coincided with the end of the LCE.

Because of the meridionally narrow extent of *u'* and *T'* as they first propagate over the Indian Ocean, considering composites of variables over a narrow range of latitudes near the equator may aid in MJO identification and prediction.

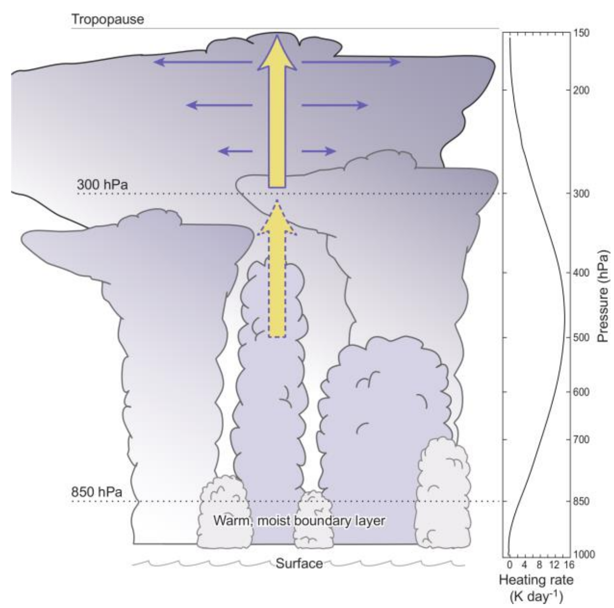

Figure 5: Schematic relating the cloud population during a convectively active MJO event to large-scale anomalies of upper-level divergence and upward motion. Large anvil clouds represent broad stratiform regions with embedded convective elements, and smaller clouds represent shallow, deep, and wide convective cores. Yellow arrows represent large-scale upward motion, and purple arrows depict large-scale divergence. The latent heating profile on the right is described in the text.

5. CONCLUSIONS

Powell and Houze (2013) showed that a cloud-humidity feedback known as "discharge-recharge" was not responsible for onset of MJO-related convection during the DYNAMO and AMIE field campaigns. Rawinsonde data in that study showed 25-30 day variability in upper-tropospheric zonal wind, temperature, and humidity anomalies. Using TRMM PR and ERA-Interim reanalysis, we have shown that the evolution of the depths of precipitating convective echoes and the structure and evolution of dynamic and thermodynamic fields observed near Gan Island are representative of the same within a much larger domain in the central equatorial Indian Ocean. As such, we are able to use the reanalysis data to extend our interpretation of rawinsonde data results to three dimensions. This allows us to study the propagation characteristics of large-scale upper-tropospheric dynamic and thermodynamic features.

Anomalies of 150 hPa zonal wind and 300 hPa temperature are generally low-wavenumber features that have eastward phase speeds and project well onto an equatorial Kelvin wave mode. Prior to MJO onset, the anomalies propagate eastward at about 15 m s^{-1}, and after convective onset their phase speeds decrease. Many prior studies have argued that one MJO event may excite a Kelvin wave that circumnavigates and becomes involved in generating the next MJO event. Straub (2013) extends this idea by noting that almost all

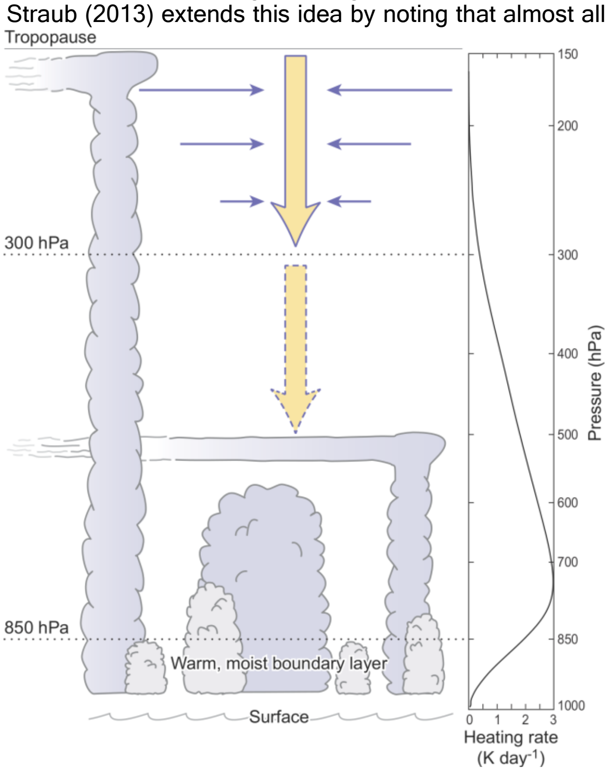

Figure 6: As in Figure 5, except for suppressed conditions beneath large-scale convergence and downward motion. Small clouds represent shallow convection, and long streamers depict long-lived anvil clouds or remnants of old anvils.

MJO convective events have some—perhaps high-wavenumber—precursor signal in upper-level zonal wind even if no circumnavigating feature is apparent. Because the meridional component of the circulation anomaly is very small, the velocity potential anomaly, and thus divergent anomaly, is dominated by the zonal wind anomaly.

Equatorial wave dynamics of various spatial and time scales have been argued to have an effect on convection during DYNAMO. Zuluaga and Houze (2013) observed 2-6 day variability in precipitation near Gan during active MJO periods, and they attributed the variability to inertia-gravity waves and possibly mixed Rossby-gravity waves and/or synoptic scale easterly waves. Other variability on the time scale of several days has been linked to high wavenumber Kelvin waves (Johnson and Ciesielski 2013) and Rossby like disturbances (Kerns and Chen 2014). Powell and Houze (2013) showed that the cloud population at a location experiencing a lull between rainfall events during an active MJO was similar to that during widespread convectively suppressed periods.

We thus propose that the large-scale Kelvin wave signal observed during DYNAMO is responsible for the 25-30 day variability in convection observed. However, the signal is clearly confined to the upper troposphere, and to date, no mechanism linking upper tropospheric dynamics to widespread convective organization has been proposed. Studies such as Barnes and Houze (2013), Powell and Houze (2013), and Yuan and Houze (2013) show that stratiform clouds are essential elements in the cloud population during a convectively active MJO event. The stratiform elements provide a source of deep diabatic heating, which generates a Kelvin-Rossby type circulation response as seen in Gill (1980). This anomalous circulation structure is observed during DYNAMO and may be partially responsible for propagating the convective envelope eastward (Kerns and Chen 2014). Shallow heating cannot produce such a realistic structure. Thus, widespread stratiform elements are unique cloud elements within an MJO and are necessary for its maintenance. Takayabu et al. (2010) demonstrated that the depth of organized deep convection is bounded by large-scale subsidence. We propose that large-scale rising (sinking) motion associated with divergence (convergence) in the upper-troposphere enhances (suppresses) the formation of large, organized stratiform regions. During DYNAMO, the divergent anomalies are associated with a low-wavenumber planetary-scale equatorial Kelvin wave. We do not yet have the capability to measure vertical velocity on the large scale, but upper-level subsidence is thought to occur beneath upper-tropospheric convergence (Kiladis et al. 2009). Furthermore, upper-tropospheric dynamics are known to impact the ability of convection to develop elsewhere in the tropics (Holland and Merrill 1984, Montgomery and Farrell 1993) and in the mid-latitudes (Sutcliffe 1939). While upper-level divergence was controlled by an equatorial Kelvin wave during DYNAMO, any long-lived feature providing upper-tropospheric divergence over the Indian Ocean or tropical west Pacific, where warm sea surface temperatures can support widespread convection, could potentially support MJO onset.

Figures 5 and 6 illustrate the relationship between the cloud population and upper level divergence and vertical motion. During enhanced periods (Fig. 5), a large variety of clouds are present. Large anvils represent broad stratiform regions that contain embedded convective elements of various depths. Smaller clouds represent wide convective cores or shallow convection. The heating rate on the right of Fig. 5 is adapted from the idealized heating rates of Schumacher et al. (2004) assuming 40% stratiform, 50% deep convective, and 10% shallow convective precipitation and a rain rate of 10 mm day^{-1}, which was typical during active MJO periods during DYNAMO (Powell and Houze 2013). Figure 6 represents the cloud population and anomalous convergence/vertical motion during convectively suppressed periods. More shallow convective echoes are present, but virtually no large stratiform areas are observed. A few wide convective cores are observed, and an occasional isolated convective element becomes very deep. The relative proportions and sizes of clouds are drawn to be consistent with Barnes and Houze (2013) and Powell and Houze (2013). The heating profile in Fig. 6 assumes 50% deep convective and 50% shallow convective precipitation and a rain rate of 3 mm day^{-1}.

Ongoing work includes using regional modeling tools to determine the impact of eastward propagating zonal wind anomalies by filtering them out of the model's boundary conditions. We will then compare the time series of rainfall for simulations including and excluding the upper-tropospheric circulation anomalies. Modeling studies will also quantify the transport of water into the middle and upper troposphere and the relative roles of cloud moistening and advective moistening processes in tropospheric humidification observed during the days prior to MJO convective onset.

Acknowledgments: S. Powell was supported by the Department of Energy under grant DOE-SC0008452.

REFERENCES

Adames, Á., and J. M. Wallace, 2014: Three-dimensional structure and evolution of the MJO and its relation to the mean flow, *J. Atmos. Sci.*, in press.

Awaka, J., T. Iguchi, H. Kumagai, and K. Okamoto, 1997: Rain type classification algorithm for TRMM precipitation radar, *Proc. 1997 Int. Geoscience and Remote Sensing Symp.*, Singapore, IEEE, 1633-1635.

Barnes, H. C., and R. A. Houze, Jr., 2013: The precipitating cloud population of the Madden-Julian Oscillation over the Indian and west Pacific oceans, *J. Geophys. Res.,* **118**, 6996-7023, doi:10.1002/jgrd.50375

Benedict, J. J., and D. A. Randall, 2007: Observed characteristics of the MJO relative to maximum rainfall, *J. Atmos. Sci.,* **64**, 2332-2354.

Bladé, I., and D. L. Hartmann, 1993: Tropical intraseasonal oscillations in a simple nonlinear model, *J. Atmos. Sci.*, **50**, 2922-2939.

Dee, D. P., and Coauthors, 2011: The ERA-Interim reanalysis: configuration and performance of the data assimilation system, *Q. J. R. Meteorol. Soc.*, **137**, 553-597.

Frierson, D. M. W., 2007: Convectively coupled Kelvin waves in an idealized moist general circulation model, *J. Atmos. Sci.*, **64**, 2076-2090.

Gill, A. E., 1980: Some simple solutions for heat-induced tropical circulation, *Q. J. R. Meteorol. Soc.*, **106**, 447-462.

Gottschalck, J., P. E. Roundy, C. J. Schreck III, A. Vintzileos, and C. Zhang, 2013: Large-scale atmospheric and oceanic conditions during the 2011-2012 DYNAMO field campaign, *Mon. Wea. Rev.*, **141**, 4173-4196.

Gray, W. M., 1973: Cumulus convection and larger scale circulations I. Broadscale and mesoscale considerations. *Mon. Wea. Rev.*, **101**, 839-855.

Holland, G. J., and R. T. Merrill, 1984: On the dynamics of tropical cyclone structural changes, *Q. J. R. Meteorol. Soc.*, **110**, 723-745.

Houze, R. A., Jr., D. C. Wilton, and B. F. Smull, 2007: Monsoon convection in the Himalayan region as seen by the TRMM precipitation radar, *Quart. J. Roy. Meteor. Soc.*, **133**, 1389-1411.

Johnson, R. H., and P. E. Ciesielski, 2013: Structure and properties of Madden-Julian oscillations deduced from DYNAMO sounding arrays, *J. Atmos. Sci.*, **70**, 3157-3179.

Kemball-Cook, S. R., and B. C. Weare, 2001: The onset of convection in the Madden-Julian oscillation, *J. Clim.*, **14**, 780-793.

Kerns, B. W. and S. S. Chen, 2014: Equatorial dry air intrusion and related synoptic variability in MJO initiation during DYNAMO. *Mon. Wea. Rev.* doi:10.1175/MWR-D-13-00159.1, in press.

Kiladis, G. N., K. H. Straub, P. T. Haertel, 2005: Zonal and vertical structure of the Madden-Julian oscillation, *J. Atmos. Sci.*, **62**, 2790-2809.

—, M. C. Wheeler, P. T. Haertel, K. H. Straub, and P. E. Roundy, 2009: Convectively coupled equatorial waves. *Rev. Geophys.*, **47**, RG2003, doi:10.1029/2008RG000266.

Knutson, R. R., and K. M. Weickmann, 1987: 30-60 day atmospheric oscillations: Composite life cycles of convection and circulation anomalies, *Mon. Weather Rev.*, **115**, 1406-1436.

Kummerow, C., W. Barnes, T. Kozu, J. Shiue, and J. Simpson, 1998: The Tropical Rainfall Measuring Mission (TRMM) sensor package, *J. Atmos. Oceanic Technol.*, **15**, 809-817.

Madden, R. A., and P. R. Julian, 1971: Detection of a 40-50-day oscillation in the zonal wind in the tropical Pacific, *J. Atmos. Sci.*, **28**, 702-708.

—, and —, 1972: Description of global-scale circulation cells in the tropics with a 40-50 day period, *J. Atmos. Sci.*, **29**, 1109-1123.

Matthews, A. J., 2008: Primary and successive events in the Madden-Julian oscillation, *Q. J. R. Meteorol. Soc.*, **134**, 439-453.

Montgomery, M. T., and B. F. Farrell, 1993: Tropical cyclone formation, *J. Atmos. Sci.*, **50**, 285-310.

Nogués-Paegle, J., B.-C. Lee, and V. E. Kousky, 1989: Observed modal characteristics of the intraseasonal oscillation, *J. Clim.*, **2**, 496-507.

Powell, S. W., and R. A. Houze, Jr., 2013: The cloud population and onset of the Madden-Julian oscillation over the Indian Ocean during DYNAMO-AMIE, *J. Geophys. Res. Atmos.,* **118**, 11,979-11,995, doi:10.1002/2013JD020421.

Schumacher, C., R. A. Houze, Jr., and I. Kraucunas, 2004: The tropical dynamical response to latent heating estimates derived from the TRMM precipitation radar, *J. Atmos. Sci.*, **61**, 1341-1358.

Seo, K-H., and K-Y. Kim, 2003: Propagation and initiation mechanisms of the Madden-Julian oscillation, *J. Geophys. Res.*, **108**(D13), 4384, doi:10.1029/2002JD002876,2003.

Straub, K. H., 2013: MJO initiation in the real-time multivariate MJO index, *J. Climate*, **26**, 1130-1151.

Sutcliffe, R. C., 1939: Cyclonic and anticyclonic development, *Q. J. Roy. Meteor. Soc.*, **65**, 518-524.

Takayabu, Y. N., S. Shige, W.-K. Tao, and N. Hirota, 2010: Shallow and deep latent heating modes over tropical oceans observed with TRMM PR spectral latent heating data, *J. Climate*, **23**, 2030-2046.

Ventrice, M. J., M. C. Wheeler, H. H. Hendon, C. J. Schreck III, C. D. Thorncroft, and G. N. Kiladis, 2013: A modified multivariate Madden-Julian oscillation index using velocity potential. *Mon. Wea. Rev.*, **141**:12, 4197-4210.

Wheeler, M. C., and K. M. Weickmann, 2001: Real-time monitoring and prediction of modes of coherent synoptic to intraseasonal tropical variability, *Mon. Wea. Rev.*, **129**, 2677-2694.

—, and H. H. Hendon, 2004: An all-season real-time multivariate MJO index: Development of an index for monitoring and prediction, *Mon. Weather Rev.*, **132**, 1917-1932.

Yoneyama, K., C. Zhang, and C. N. Long, 2013: Tracking pulses of the Madden-Julian Oscillation. *Bull. Am. Meteorol. Soc.*, **94**, 1871-1891.

Yuan, J., and R. A. Houze, Jr., 2013: Deep convective systems observed by A-Train in the tropical Indo-Pacific region affected by the MJO, *J. Atmos. Sci.*, **70**, 465-486.

Zhang, C., 2005: Madden-Julian oscillation, *Rev. Geophys.*, **43**, RG2003, doi:10.1029/2004RG000158.

Zuluaga, M. D., and R. A. Houze, Jr., 2013: Evolution of the population of precipitating convective systems over the equatorial Indian Ocean in active phases of the Madden-Julian oscillation, *J. Atmos. Sci.,* **70***,* 2713-2725.